

# New spectral characterization of dimethyl ether isotopologues $\text{CH}_3\text{OCH}_3$ and $^{13}\text{CH}_3\text{OCH}_3$ in the THz region

J.M. Fernández and G. Tejada

Laboratory of Molecular Fluid Dynamics, Instituto de Estructura de la Materia  
IEM-CSIC, Unidad Asociada GIFMAN, CSIC-UHU; 28006 Madrid, Spain;

`jm.fernandez@csic.es`

and

M. Carvajal

Dpto. Ciencias Integradas, Centro de Estudios Avanzados en Física, Matemática y  
Computación, Facultad de Ciencias Experimentales, Universidad de Huelva; Unidad  
Asociada GIFMAN, CSIC-UHU; 21071 Huelva, Spain

Instituto Universitario Carlos I de Física Teórica y Computacional, Universidad de  
Granada, Granada, Spain

and

M.L. Senent

Theoretical Chemistry and Physics Department, Instituto de Estructura de la Materia  
IEM-CSIC, Unidad Asociada GIFMAN, CSIC-UHU; 28006 Madrid, Spain;

Received \_\_\_\_\_; accepted \_\_\_\_\_

## ABSTRACT

The torsional Raman spectra of two astrophysically detected isotopologues of dimethyl-ether, ( $^{12}\text{CH}_3\text{O}^{12}\text{CH}_3$  and  $^{13}\text{CH}_3\text{O}^{12}\text{CH}_3$ ), have been recorded at room temperature and cooled in supersonic jet, and interpreted with the help of highly correlated ab initio calculations. Dimethyl-ether displays excited torsional and vibrational levels at low energy that can be populated at the temperatures of the star forming regions, obliging to extend the analysis of the rotational spectrum over the ground state. Its spectrum in the THz region is rather complex due to the coupling of the torsional overtones  $2\nu_{11}$  and  $2\nu_{15}$  with the COC bending mode, and the presence of many hot bands. The torsional overtones are set here at  $2\nu_{11} = 385.2 \text{ cm}^{-1}$  and  $2\nu_{15} = 482.0 \text{ cm}^{-1}$  for  $^{12}\text{CH}_3\text{O}^{12}\text{CH}_3$ , and  $2\nu_{11} = 385.0 \text{ cm}^{-1}$  and  $2\nu_{15} = 481.1 \text{ cm}^{-1}$  for  $^{13}\text{CH}_3\text{O}^{12}\text{CH}_3$ . The new assignment of  $2\nu_{11}$  is downshifted around  $\sim 10 \text{ cm}^{-1}$  with respect to the literature. All the other (hot) bands have been re-assigned consistently. In addition, the infrared-forbidden torsional fundamental band  $\nu_{11}$  is observed here at  $197.8 \text{ cm}^{-1}$ . The new spectral characterization in the THz region reported here provides improved values of the Hamiltonian parameters, to be used in the analysis of the rotational spectra of DME isotopologues for further astrophysical detections.

*Subject headings:* astrochemistry - molecular data - methods: laboratory: molecular - techniques: spectroscopic - ISM: lines and bands - ISM: molecules

## 1. Introduction

Dimethyl ether (DME,  $\text{CH}_3\text{OCH}_3$ ) is a relevant astrophysical molecule which was first detected in the ISM by Snyder et al. (1974), and later on, identified as an abundant species in star forming regions (Schilke et al. 2001). DME is mainly formed in the gas phase via the radiative association reaction of methoxy and methyl radicals, and it presents a correlation with methyl formate (Carvajal et al. 2010; Favre et al. 2014), via the oxidation of  $\text{CH}_3\text{OCH}_2$ , in cold objects (Balucani et al. 2015).

In addition to works prior to its detection in the ISM (Taylor & Vidale 1957; Kasai & Myers 1959; Fateley & Miller 1962; Blukis et al. 1963; Durig et al. 1976; Groner & Durig 1977), the astrophysical interest for the complete description of the spectrum in the millimeter and submillimeter regions of DME and its isotopologues, such as  $^{13}\text{CH}_3\text{OCH}_3$  ( $^{13}\text{C}$ -DME) and  $\text{CH}_3\text{OCH}_2\text{D}$  (d-DME), has brought about many laboratory studies of its rotational spectrum and of a few vibrational bands (Lovas et al. 1979; Neustock et al. 1990; Groner et al. 1998; Coudert et al. 2002; Niide & Hayashi 2003; Endres et al. 2009; Kutzer et al. 2016). In turn, the analysis of an extensive number of spectral lines in astronomical observations has given rise to the identification of DME in Orion-KL (Brouillet et al. 2013) and the detection of the first excited torsional states lines in a high-mass star forming region (Bisschop et al. 2013). Furthermore, the ground state rotational lines corresponding to the monosubstituted isotopologues  $^{13}\text{C}$ -DME and d-DME were first observed in a high-mass star forming region (Koerber et al. 2013; Richard et al. 2013).

DME is a non-rigid asymmetric-top with two methyl internal rotors that splits each rovibrational level into nine components (Groner & Durig 1977; Senent et al. 1995a,b), some of them degenerate. Hence, the high-resolution spectrum of DME is quite dense and its analysis challenging. Furthermore, because the first and the second excited torsional levels lie at relatively low energy, they can be populated at the temperatures of the hot core

regions obliging to extend the spectral analysis to the two torsional fundamentals and their overtones. The spectral region of the torsional overtones is further complicated due to their coupling with the COC bending mode (Senent et al. 1995b), and the presence of many hot bands. The following notation will be used throughout the paper:  $\nu_{11}$  is the “anti-gearred” torsion,  $\nu_{15}$  the “geared” torsion, and  $\nu_7$  the COC bending mode; vib-torsional energy levels will be denoted as  $(v_{11} v_{15} v_7)$ , where  $v_n$  is the number of torsional or vibrational quanta in the corresponding mode.

The torsional spectrum of DME was explored experimentally at room temperature by Groner & Durig (1977), using Raman and infrared techniques. The torsional fundamental  $\nu_{15}$  was observed at  $241.0 \text{ cm}^{-1}$ . The other torsional fundamental  $\nu_{11}$  is forbidden in the absorption spectrum, and was estimated between  $199 \text{ cm}^{-1}$  and  $202 \text{ cm}^{-1}$ . The two torsional overtones were assigned to the peaks observed at  $2\nu_{11} = 395.5 \text{ cm}^{-1}$  and  $2\nu_{15} = 481.2 \text{ cm}^{-1}$ . The lack of an accurate value for the  $\nu_{11}$  torsional mode, prevented the determination of some of the interaction parameters of the effective Hamiltonian, needed for further analysis.

In this paper, the torsional Raman spectra of DME and of  $^{13}\text{C}$ -DME have been recorded at room temperature, and of cooled DME in supersonic jet. The spectrum of cooled DME allowed us to assign unequivocally the torsional overtones and their first hot bands, amending some of the previous assignments. In turn, the new frequencies have been used to refine 3D quantum calculations employing state-of-the art CCSD(T) ab initio calculations (Villa et al. 2011) and a torsion-torsion-bending Hamiltonian (Senent et al. 1995b; Carvajal et al. 2012). The new characterization provides improved values of the Hamiltonian parameters for the analysis of DME and  $^{13}\text{C}$ -DME rotational spectra and future astrophysical detections.

## 2. New experimental Raman measurements

Two sets of Raman spectra of DME were recorded in this work: i) at room temperature, and ii) jet-cooled. The sample of DME was supplied by PRAXAIR, nominal purity 99.8 %, while that of  $^{13}\text{C}$ -DME was synthesized in the University of Kassel, Germany (Kutzer et al. 2016); the latter sample was distilled by liquid nitrogen to remove residual  $\text{H}_2$  from the synthesis. Raman spectra of DME and of  $^{13}\text{C}$ -DME were recorded at room temperature under static conditions (pressure 550 mbar and 380 mbar, respectively). In addition, supersonic jets of mixtures of DME diluted in He were produced, to cool the DME. Raman shifts were calibrated against Hg and Ne emission lines, and are accurate to  $\pm 0.1 \text{ cm}^{-1}$ . Raman scattering was excited by 10 W of linearly polarized radiation at 532 nm from a Coherent Verdi V10 laser, sharply focused down to a  $15 \mu\text{m}$  beam waist on the sample by a  $f=35 \text{ mm}$  lens. Scattered radiation perpendicular to both laser propagation and polarization was collected by an  $f=55 \text{ mm}$  photographic objective (Nikon,  $f/1.8$ ) and projected, with a total magnification  $\times 10$ , onto the entrance slit of the spectrograph. This is a Jobin-Yvon double monochromator, equipped with two 2400 groove/mm gratings, and a CCD detector with  $13 \times 13 \mu\text{m}^2$  pixels, refrigerated by liquid nitrogen. Entrance slit was 75 and  $150 \mu\text{m}$ , yielding spectral resolution of 0.36 and  $0.72 \text{ cm}^{-1}$ , respectively. Several scans were spike-filtered and averaged.

Raman spectroscopy can be an invaluable tool to investigate the torsional modes of symmetric molecules like ethane (Fantoni et al. 1986; Fernández-Sánchez et al. 1989), propane (Engeln et al. 1990), or butane (Compton et al. 1980; Engeln & Reuss 1991). In such symmetric molecules, some of the torsional modes are forbidden in IR or MW absorption, while the torsional overtones give rise to weak Q-branches in Raman spectrum, often accompanied by a rich structure of hot bands. In the case of DME, the  $\nu_{11}$  torsional mode is silent in IR-MW; on the contrary, the two torsional modes are Raman allowed, as

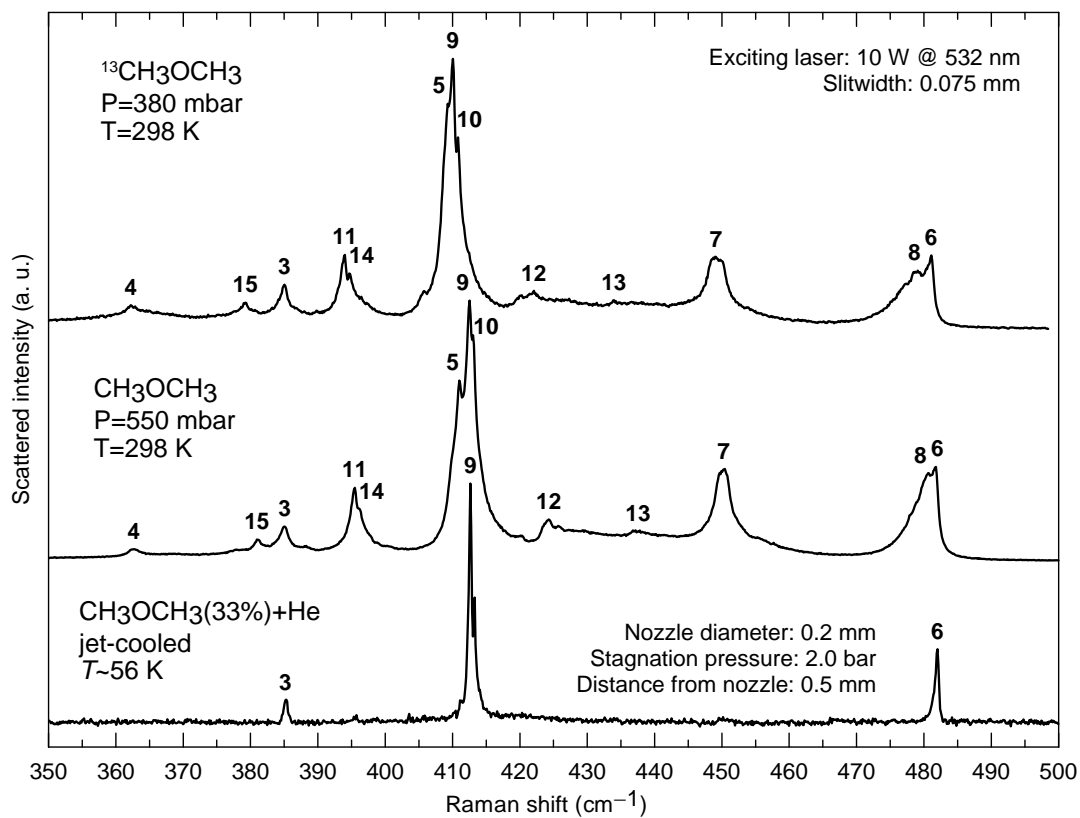


Fig. 1.— Raman spectrum of CH<sub>3</sub>OCH<sub>3</sub> and <sup>13</sup>CH<sub>3</sub>OCH<sub>3</sub> in the region of the torsional overtones. Band numbering refer to Table 2 (Appendix).

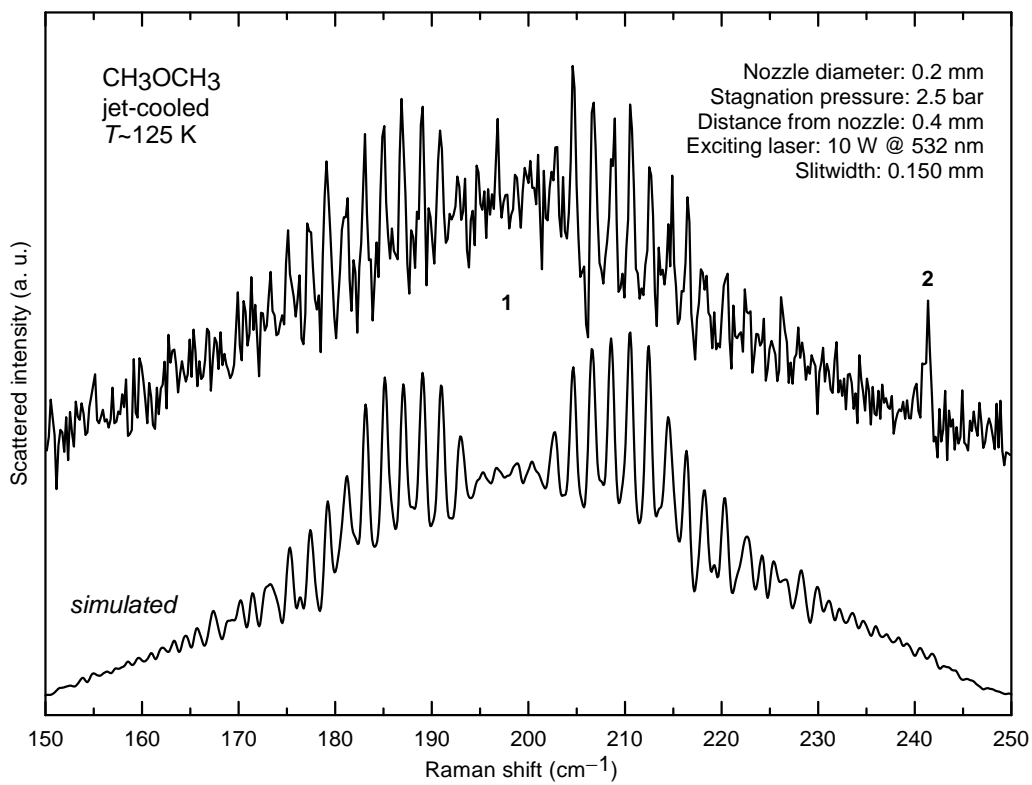


Fig. 2.— Raman spectrum of jet-cooled CH<sub>3</sub>OCH<sub>3</sub> in the region of the torsional fundamentals. Band numbering refer to Table 2 (Appendix).

well as their overtones. The Raman spectra of DME and  $^{13}\text{C}$ -DME in this latter region is shown in Fig. 1. This region is dominated by the COC bending mode  $\nu_7$ , which yields the peak at  $\sim 410\text{ cm}^{-1}$ . In addition to that, a rich structure of peaks due to hot bands can be seen, what difficults the safe assignment of the two torsional overtones. The spectrum of  $^{13}\text{C}$ -DME is rather similar to that of DME, with some of the peaks shifted towards lower wavenumbers, due to the mass increase, as discussed below. The lowest panel shows the spectrum of jet cooled DME in a supersonic expansion diluted in helium. It can be clearly seen that at low temperature, only three peaks survive, which can be assigned unambiguously to the two torsional overtones plus the COC bending modes. Actually, the  $2\nu_{11}$  torsional overtone had been wrongly assigned (Groner & Durig 1977) to the peak at  $395.5\text{ cm}^{-1}$  in the room temperature spectrum, which dissapears when the molecule is jet-cooled, while the peak at  $385.2\text{ cm}^{-1}$  remains at low temperature.

The Raman spectrum of the jet-cooled DME in the region of the torsional fundamentals is shown in Fig. 2. These Raman bands are extremely weak, and had not been reported before. The faint Q-branch at  $241.4\text{ cm}^{-1}$  is the  $\nu_{15}$  mode, which was observed previously in IR (Fateley & Miller 1962; Groner & Durig 1977). The broad band with the comb-like rotational structure can be assigned to the unobserved  $\nu_{11}$  torsional fundamental. A simulation with PGOPHER (Western 2016), with the selection rules  $\Delta K_a = \pm 1$  and  $\Delta K_c = \pm 1$ , corresponding to a Raman band of  $A_2$  symmetry in the  $C_{2v}$  point group, allows to locate the band origin at  $197.8\text{ cm}^{-1}$ , although it could be downshifted by one unit of the peak spacing ( $1.9\text{ cm}^{-1}$ ).

### 3. Theoretical model for the spectral analysis

In previous papers on DME (Villa et al. 2011) and its isotopologues  $\text{CH}_3\text{OCD}_3$  and  $\text{CD}_3\text{OCD}_3$  (Senent et al. 2012),  $^{13}\text{CH}_3\text{OCH}_3$  (Carvajal et al. 2012), and  $\text{CH}_3\text{OCH}_2\text{D}$  (Car-

vajal et al. 2014), we used a three-dimensional (3D) model for the analysis of their far infrared spectra. Assuming that the three low-frequency vibrational modes can be treated separately from the remaining “high-frequency” vibrations, the 3D-Hamiltonian can be written as:

$$\hat{H}(\alpha, \theta_1, \theta_2) = - \sum_{i=1}^3 \sum_{j=1}^3 \frac{\partial}{\partial q_i} B_{ij}(\alpha, \theta_1, \theta_2) \frac{\partial}{\partial q_j} + V^{\text{eff}}(\alpha, \theta_1, \theta_2) \quad (1)$$

In this equation,  $q_i, q_j = (\alpha, \theta_1, \theta_2)$  represent the three independent variables: the COC bending  $\alpha$  and the two torsional coordinates  $\theta_1, \theta_2$ . The first term, which depends on the  $B_{ij}$  parameters (the G matrix elements in  $\text{cm}^{-1}$ ), is a 3D-kinetic energy operator. The second term, the effective potential energy  $V^{\text{eff}}$ , is the sum of three contributions

$$V^{\text{eff}}(\alpha, \theta_1, \theta_2) = V(\alpha, \theta_1, \theta_2) + V'(\alpha, \theta_1, \theta_2) + V^{\text{ZPVE}}(\alpha, \theta_1, \theta_2) \quad (2)$$

where  $V(\alpha, \theta_1, \theta_2)$  is the ab initio potential energy,  $V'(\alpha, \theta_1, \theta_2)$  the Podolsky pseudopotential, and  $V^{\text{ZPVE}}(\alpha, \theta_1, \theta_2)$  the zero point vibrational energy correction. The ab initio potential energy  $V$  is isotopically invariant, whereas  $V'$  and  $V^{\text{ZPVE}}$  (and thus the effective potential  $V^{\text{eff}}$ ) depend on the nuclear masses, as well as, of course, the kinetic energy parameters  $B_{ij}$ .

All the terms in Eqs. (1) and (2) can be determined from energies, geometries, and harmonic frequencies from accurate ab initio calculations, as described elsewhere (Senent 1998a,b). In the present paper, we used the previous ab initio calculations by Villa et al. (2011), performed with the Gaussian 09 code (Frisch et al. 2009). Coupled-cluster theory with single and double substitutions (CCSD) (Scuseria & Schaefer III 1989) was employed for the geometry optimizations. To improve the energies, single point calculations were performed adding a perturbative treatment of triple excitations (CCSD(T)) (Pople et al. 1987) on the CCSD geometries. Long range effects are well described because the augmented aug-cc-pVTZ basis set was employed in all the computations (Woon & Dunning 1993).

Ab initio energies  $V(\alpha, \theta_1, \theta_2)$  were calculated at 126 configurations for selected values of the three  $(\alpha, \theta_1, \theta_2)$  coordinates:  $\alpha = (104.676^\circ \rightarrow 119.676^\circ, \Delta\alpha = 3^\circ)$ , and  $\theta_1, \theta_2 = 0, \pm 30, \pm 90, \pm 150, 180$  degrees. In all the 126 configurations, the remaining  $3N - 9$  internal coordinates were allowed to relax. The other terms of the Hamiltonian,  $B_{ij}$ ,  $V'$ , and  $V^{\text{ZPVE}}$ , were also computed for the same 126 configurations; the  $V^{\text{ZPVE}}$  correction, needed to obtain reliable results (Smeyers et al. 1996), was computed within the harmonic approximation. Analytical 3D effective potential energy surfaces  $V^{\text{eff}}(\alpha, \theta_1, \theta_2)$  for DME and  $^{13}\text{C}$ -DME were then obtained by fitting their values at the 126 configurations to a series of the form

$$V^{\text{eff}}(\alpha, \theta_1, \theta_2) = \sum_{l=0}^3 \left[ \sum_{m=0}^2 \sum_{n=0}^2 A_{lmn} \alpha^l \cos(3m\theta_1) \cos(3n\theta_2) + B_{l11} \alpha^l \sin(3\theta_1) \sin(3\theta_2) \right] \quad (3)$$

For DME,  $A_{lmn} = A_{lnm}$  and  $B_{lmn} = B_{lnm}$ , while for the less symmetric  $^{13}\text{C}$ -DME, the  $|A_{lmn} - A_{lnm}|$ , and  $|B_{lmn} - B_{lnm}|$  differences are found to be lower than  $0.0001 \text{ cm}^{-1}$ . Formally identical fits were carried out for each of the kinetic energy operators  $B_{ij}(\alpha, \theta_1, \theta_2)$ .

The original code ENEDIM (Senent 2001) was used to carry out the calculations and fits of the  $V^{\text{eff}}(\alpha, \theta_1, \theta_2)$  and  $B_{ij}(\alpha, \theta_1, \theta_2)$  surfaces, and then to compute variationally the torsional and bending energy levels of the 3D Hamiltonian. To reduce the computational expenses and for the classification of the levels, the molecular symmetry properties were taken into consideration. The two isotopologues studied here,  $^{12}\text{CH}_3\text{O}^{12}\text{CH}_3$  (DME) and  $^{13}\text{CH}_3\text{O}^{12}\text{CH}_3$  ( $^{13}\text{C}$ -DME), can be classified in the  $G_{36}$  and  $G_{18}$  Molecular Symmetry Groups (Bunker & Jensen 1989), respectively.  $G_{36}$  contains nine irreducible representations: four non-degenerate  $A_1$ ,  $A_2$ ,  $A_3$ , and  $A_4$ , four doubly-degenerate  $E_1$ ,  $E_2$ ,  $E_3$ , and  $E_4$  and one four-fold degenerate G.  $G_{18}$  contains two non-degenerate representations  $A_1$  and  $A_2$  and four double-degenerate ones  $E_1$ ,  $E_2$ ,  $E_3$ , and  $E_4$ . The correlation between  $G_{36}$  and  $G_{18}$  representations was detailed in previous papers (Carvajal et al. 2012; Villa et al. 2013).

In our previous papers (Villa et al. 2011; Carvajal et al. 2014), the parameters of the

ab initio Hamiltonian were refined to reproduce the old available experimental frequencies of Groner & Durig (1977). In the present work, the refinement has been revisited using the new Raman observations, as described in the next section. We can anticipate that the ab initio calculations are closer to the new experimental data than to the old ones.

#### 4. Discussion

The new Raman spectra of cooled DME reported here (see Figs. 1 and 2) probed crucial for the right assignment of the torsional modes and their overtones. At  $T = 56$  K, only three bands survive in the recorded Raman spectrum of DME in the bottom trace of Fig. 1. At such low  $T$ , only transitions starting from the ground state (000) can be observed, due to the population distribution. Thus, the observed 3 peaks can be safely assigned to the transitions from ground state to the (200), (001) and (020) levels, respectively. This has allowed us to reassign the torsional overtone (200) and, with the help of the ab initio calculations, to amend the assignment of other bands already reported in both infrared and Raman spectra. In fact, Groner & Durig (1977) proposed that the torsional overtone (200) of DME lie at  $395.5\text{ cm}^{-1}$  and its first hot band (100) $\rightarrow$ (300) at  $385.0\text{ cm}^{-1}$  whereas, in this work, they are set at  $385.2\text{ cm}^{-1}$  and  $362.6\text{ cm}^{-1}$ , respectively. These new assignments are downshifted by around  $\sim 10\text{ cm}^{-1}$  and  $\sim 22\text{ cm}^{-1}$  with respect to those by Groner & Durig (1977). The peak around  $395\text{ cm}^{-1}$  is assigned here to two overlapping hot bands of the  $\nu_7$  bending: (010) $\rightarrow$ (011) and (001) $\rightarrow$ (002). The remaining prominent feature at  $\sim 450\text{ cm}^{-1}$  in Fig. 1, unassigned in Groner & Durig (1977), is the hot band (100) $\rightarrow$ (120).

The complete lists of the experimental wavenumbers for both DME and  $^{13}\text{C}$ -DME, along with their assignments and calculated torsional splittings, are displayed in Table 2 (Appendix). The accuracy of the reported wavenumbers is mainly determined by the line shape, as a result of the (unresolved) rotational structure and/or torsional splittings. Thus,

the quoted uncertainties range from  $\pm 0.2 \text{ cm}^{-1}$  for isolated narrow bands up to  $\pm 0.5 \text{ cm}^{-1}$  for broad, overlapped, or weak bands. As a representative check, the (001) bending energy levels, observed here at  $412.5 \text{ cm}^{-1}$  for DME and  $410.0 \text{ cm}^{-1}$  for  $^{13}\text{C}$ -DME, are consistent within experimental error with the more accurate values ( $412.350 \text{ cm}^{-1}$  and  $409.993 \text{ cm}^{-1}$ ) reported recently by Kutzer et al. (2016).

It is worth to discuss the isotopic shifts, from DME to  $^{13}\text{C}$ -DME, of the peaks in Fig. 1 in light of this new assignment. The larger isotopic shifts ( $\sim 2.5 \text{ cm}^{-1}$ ) are those of the COC bending mode (and their overtones and combinations), which are directly affected by the increased mass of one of the C atoms. On the contrary, in zeroth-order approximation, the torsional modes, (due to the internal rotation of the two methyl groups) should not be affected by the mass of the C atoms, because they lie on the rotation axis, and thus do not contribute to the rotor moment of inertia. Of course, coupling between the bending and the torsional modes leads to the observed isotopic shifts of the torsional overtones. The  $\nu_{15}$  mode is more strongly coupled to the bending of the COC skeletal frame (as revealed by its higher frequency and intensity) than the  $\nu_{11}$  mode. Thus, the new assignment proposed here is further supported by the tiny isotopic shift ( $0.2 - 0.4 \text{ cm}^{-1}$ ) of the peaks involving  $\nu_{11}$ , as opposed to those ( $\sim 1 \text{ cm}^{-1}$ ) involving  $\nu_{15}$ .

To obtain the best fit parameters of the effective Hamiltonian, we started from the ab initio potential energy surfaces and the ab initio kinetic parameters calculated in our previous works on DME (Villa et al. 2011) and  $^{13}\text{C}$ -DME (Carvajal et al. 2012). Those ab initio calculations provided a reasonable description of the torsional features but failed to reproduce the bending fundamental  $\nu_7$  ( $421.64 \text{ cm}^{-1}$  ab initio vs  $412.35 \text{ cm}^{-1}$  observed by Kutzer et al. (2016)). The ab initio Hamiltonian was then refined in this work following three steps: i) the adjustment of the bending fundamental close to the experimental value; ii) the reassignment of the two torsional fundamentals and their overtones according to the

new Raman spectra; iii) the assignment of the other observed bands and the subsequent global fit of the Hamiltonian. The main difference, between the old Hamiltonians from Villa et al. (2011) and Carvajal et al. (2012) and the present one, involves the second step. These three steps are detailed next.

i) The main weakness of the ab initio potential energy surface (Villa et al. 2011) concerns the employed definition of the COC-bending coordinate, which was set to the COC angle  $\alpha$ , missing the contribution of other coordinates such as the in-plane HCO angles. Therefore, for a more realistic description of the COC bending, a new  $\alpha'$  coordinate was introduced

$$\alpha' = \alpha (1 + F/100) \quad , \quad (4)$$

where  $F$  is a factor which corrects the contribution of the curvilinear internal coordinate angle to the normal COC-bending coordinate. Hence, the  $B_{\alpha,\alpha}$  kinetic parameter was also corrected in all the conformations. For DME and  $^{13}\text{C}$ -DME,  $F$  was optimized to be 1.954 (Villa et al. 2011; Carvajal et al. 2012) to reproduce the experimental bending energy term values. This represents a coordinate correction lower than 2%.

ii) The ab initio torsional overtones of DME (Villa et al. 2011), when compared with the experimental data by Groner & Durig (1977), yielded the differences (obs-calc)  $\Delta = 395.5 - 388.61 = +6.89 \text{ cm}^{-1}$  for  $2\nu_{11}$ , and  $\Delta = 481.2 - 487.22 = -6.02 \text{ cm}^{-1}$  for  $2\nu_{15}$ . One torsional overtone seemed to be underestimated by the calculations whereas the other one appeared overestimated. In the subsequent adjustment (Villa et al. 2011), the potential term  $B_{011}$  in Eq. 3, one of the main responsible for the gap between  $\nu_{11}$  and  $\nu_{15}$  bands, had to be forced and strongly modified to reproduce the old data.

Here, with the new Raman reassignments, the discrepancies between experimental and ab initio values decrease significantly:  $\Delta = 385.2 - 388.61 = -3.41 \text{ cm}^{-1}$  for  $2\nu_{11}$ , and  $\Delta = 482.0 - 487.22 = -5.22 \text{ cm}^{-1}$  for  $2\nu_{15}$ . Thus, both overtones appear now at higher

frequencies in the calculations, and gaps between torsional levels are described correctly without any refinement of the  $B_{011}$  parameter.

iii) To reproduce the newly assigned experimental bands, just a few parameters of the Hamiltonian need to be optimized: one kinetic parameter and two potential parameters. In Table 3 in the Appendix the fitted effective potential coefficients ( $A_{200}$ ,  $A_{020}$ ) are indicated.

The new optimized Hamiltonians are more confident to be used in the assignments of other bands of the two isotopologues and in future works. For example, the infrared-forbidden torsional fundamental  $\nu_{11}$  of DME, calculated ab initio at  $199.16\text{ cm}^{-1}$  is predicted now at  $198.33\text{ cm}^{-1}$ , much closer to the present experimental observation at  $197.8\text{ cm}^{-1}$  (see Figure 2).

Table 1 lists the torsional-bending energies for DME and  $^{13}\text{C}$ -DME up to  $\sim 860\text{ cm}^{-1}$  calculated in this work, and compared with those reported previously. It should be stressed that the calculated energy levels could be labelled within a  $(\nu_{11}\nu_{15}\nu_7)$  scheme up to  $\sim 825\text{ cm}^{-1}$ , as listed in Table 1. For higher energies, the large torsional splittings and mixing of the wavefunctions impedes to assign unambiguously such a  $(\nu_{11}\nu_{15}\nu_7)$  label to all the computed levels, especially for the less symmetric  $^{13}\text{C}$ -DME. The experimental Raman transition wavenumbers of DME and  $^{13}\text{C}$ -DME, and their assignments, are listed in Table 2 (Appendix) to facilitate the understanding of Figures 1 and 2, along with the calculated wavenumbers from the fitted energies of Table 1.

## 5. Concluding remarks

The spectrum of DME and isotopologues in the THz region is rather complex due to the high density of states, the torsional splittings, the coupling of the torsional overtones with the COC bending mode, and the presence of many hot bands. Thus, a conclusive

assignment of the far infrared spectrum is greatly facilitated by measurements at different temperatures to distinguish between cold and hot bands. This is one of the main results of the present work.

New laboratory measurements of the torsional Raman spectrum of DME and  $^{13}\text{C}$ -DME, from room temperature down to 56 K, are reported. This has allowed us to observe the torsional band  $\nu_{11} = 197.8 \text{ cm}^{-1}$ , not reported to date, and to reassign its overtone at  $2\nu_{11} = 385.2 \text{ cm}^{-1}$  and  $385.0 \text{ cm}^{-1}$  for DME and  $^{13}\text{C}$ -DME, respectively. In due turn, this has also allowed us to assign correctly all the lowest energy levels (see Table 1), which are those relevant for the interpretation of the astronomical observations.

The new Raman measurements have been interpreted with the help of highly correlated ab initio calculations within a 3D torsional-vibrational model. The ab initio parameters of the 3D Hamiltonian have been refined using the new experimental data. In the past, such refinement stood out some problems derived from the lack of experimental data corresponding to the  $\nu_{11}$  torsional mode, and the large density of states in the region of the torsional overtones, where the coupling with the COC bending occur. These problems have been fixed here, reaching a better agreement with the experiment. Eventually, the quantitative interpretation of the energy level structure in molecules with such large amplitude internal motions relies on quantum chemical calculations validated by laboratory data.

DME has been observed in excited torsional states in hot astrophysical environments. The present results can help to the characterization of low energy states which can be responsible for unidentified lines of astrophysical surveys, where the presence of the low energy overtones can be relevant. The best fit Hamiltonian reported here can be used to verify former spectral analyses in the gas phase, and to predict other yet unobserved bands, for future astrophysical detections of other isotopologues of DME in the ISM.

This research is supported by the Spanish Ministerio de Economía y Competitividad (MINECO) under Grants FIS2014-53448-C2-2-P, FIS2016-76418-P and FIS2017-84391-C2. The authors also acknowledge the COST Actions CM1401 “Our Astrochemical History” and CM1405 “MOLIM” and CTI (CSIC) and CESGA for computing facilities. Thanks are due to Pia Kutzer and Thomas Giesen (Universität Kassel) for providing the sample of  $^{13}\text{CH}_3\text{OCH}_3$  used in this work.

## REFERENCES

- Balucani, N., Ceccarelli, C., & Taquet, V. 2015, MNRAS, 449, L16
- Bisschop, S.E., Schilke, P., Wyrowski, F., Belloche, A., Brinch, C., Endres, C.P., Gusten, R., Hafok, H., Heyminck, S., Jorgensen, J.K., Müller, H.S.P., Menten, K.M., Rolffs, R., & Schlemmer, S. 2013, A&A, 552, 122
- Blukis, U., Kasai, P.H., & Myers, R.J. 1963, JChPh, 38, 2753
- Brouillet, N., Despois, D., Baudry, A., Peng, T.-C., Favre, C., Wootten, A., Remijan, A.J., Wilson, T.L., Combes, F., & Wlodarczak, G. 2013, A&A, 550, 46
- Bunker, P. R. & Jensen, P. 1989, *Molecular Symmetry and Spectroscopy*, NRC Research Press, Ottawa.
- Carvajal, M., Kleiner, I., & Demaison, J. 2010, ApJS, 190, 315
- Carvajal, M., Álvarez-Bajo, O., Senent, M.L., Domínguez-Gómez, R., & Villa, M. 2012, JMoSp, 279, 3
- Carvajal, M., Senent, M.L., Villa, M., & Domínguez-Gómez, R. 2014, CPL, 592, 200
- Compton, D.A.C., Montero, S., & Murphy, W.F 1980, JPhCh, 84, 3587
- Coudert, L.H., Çarçabal, P., Chevalier, M., Broquier, M., Hepp, M., & Herman, M. 2002, JMoSp, 212, 203
- Durig, J.R., Li, Y.S., & Groner, P. 1976, JMoSp, 62, 159
- Endres, C.P., Drouin, B.J., Pearson, J.C., Müller, H.S.P., Lewen, F., Schlemmer, S., & Giesen T.F. 2009, A&A, 504, 635

- Engeln, R., Reuss, J., Consalvo, D., van Bladel, J.W.I., van der Avoird, A., & Pavlov-Verevkin, V. 1990, CP, 144, 81
- Engeln, R., & Reuss, J. 1991, CP, 156, 215
- Fantoni, R., van Helvoort, K., Knippers, W., & Reuss, J. 1986, CP, 110, 1
- Fateley, W.G., & Miller, F.A. 1962, AcSpe, 18, 977
- Favre, C., Carvajal, M., Field, D., Jørgensen, J.K., Bisschop, S.E., Brouillet, N., Despois, D., Baudry, A., Kleiner, I., Bergin, E.A., Crockett, N.R., Neill, J.L., Margulés, L., Huet, T.R., & Demaison, J. 2014, ApJS, 215, 25
- Fernández-Sánchez, J.M., Valdenebro, A.G., & Montero, S. 1989, JChPh, 91, 3327
- Frisch, M.J., Trucks, G.W., Schlegel, H.B., Scuseria, G.E., Robb, M.A., Cheeseman, J.R., Scalmani, G., Barone, V., Mennucci, B., Petersson, G.A. et al. 2009, Gaussian 09, Revision A.1, Gaussian, Inc., Wallingford CT
- Groner, P., & Durig, J.R. 1977, JChPh, 66, 1856
- Groner, P., Albert, S., Herbst, E., & de Lucia, F.C. 1998, ApJ, 500, 1059
- Kasai, P.H., & Myers, R.J. 1959, JChPh, 30, 1096
- Koerber, M., Bisschop, S.E., Endres, C.P., Kleshcheva, M., Pohl, R.W.H., Klein, A., Lewen, F., & Schlemmer, S. 2013, A&A, 558, 112
- Kutzer, P., Weismann, D., Wassmuth, B., Pirali, O., Roy, P., Yamada, K.M.T., Giesen, T.F. 2016 JMoSp 329, 28
- Lovas, F.J., Lutz, H., & Dreizler, H. 1979, JPCRD, 8, 1051
- Neustock, W., Guarnieri, A., Demaison, J., & Wlodarzak, G. 1990, ZNatA, 45, 702

- Niide, Y., & Hayashi, M. 2003, JMoSp, 220, 65
- Pople, J.A., Head-Gordon, M., Raghavachari, K. 1987, JChPh, 87, 5968
- Richard, C., Margulès, L., Caux, E., Kahane, C., Ceccarelli, C., Guillemin, J.-C., Motiyenko, R.A., Vastel, C., & Groner, P. 2013, A&A, 552, 117
- Schilke, P., Bendford, D.J., Hunter, T.R., Lis, D.C., & Phillips, T.G. 2001, ApJ, 132, 281
- Scuseria, G.E., & Schaefer III, H.F. 1989, JChPh, 90, 3700
- Senent, M.L., Moule, D.C., & Smeyers, Y.G. 1995, CaJPh, 73, 425
- Senent, M.L., Moule, D.C., & Smeyers, Y.G. 1995, JChPh, 102, 5952
- Senent, M.L. 1998a, JMoSp, 191, 265
- Senent, M.L. 1998b, CPL, 296, 299
- Senent, M.L. 2001, ENEDIM, A variational code for non-rigid molecules
- Senent, M.L., Domínguez-Gómez, R., Carvajal, M., & Villa, M. 2012, JPhChA, 116, 6901
- Smeyers, Y.G., Villa, M., Senent, M.L., 1996, JMoSp, 177, 66.
- Snyder, L.E., Buhl, D., Schwartz, P.R., Clark, F.O., Johnson, D.R., Lovas, F.J., & Giguere, P.T. 1974, ApJ, 191, L79
- Taylor, R.C., & Vidale, G.L. 1957, JChPh, 26, 122
- Villa, M., Senent, M.L., Domínguez-Gómez, R., Álvarez-Bajo, O., & Carvajal, M. 2011, JPhChA, 115, 13573
- Villa, M., Senent, M.L., Carvajal, M., 2013, PCCP, 15, 10258
- Western, C.M. 2016, JQSRT, 186, 221

Woon, D.E., Dunning, T.H. Jr. 1993, JChPh, 98, 1358

Table 1. Energies (in  $\text{cm}^{-1}$ ) of the lowest torsional and bending levels of DME and  $^{13}\text{C}$ -DME.

| $(v_{11} v_{15} v_7)$ | Symm. | $^{12}\text{CH}_3\text{O}^{12}\text{CH}_3$ |                  | Symm. | $^{13}\text{CH}_3\text{O}^{12}\text{CH}_3$ |                  |
|-----------------------|-------|--|------------------|-------|--|------------------|
|                       |       | OLD <sup>a</sup>                           | NEW <sup>b</sup> |       | OLD <sup>c</sup>                           | NEW <sup>b</sup> |
| 000                   | A1    | 0.000                                      | 0.000            | A1    | 0.000                                      | 0.000            |
|                       | G     | 0.000                                      | 0.000            | E1    | 0.000                                      | 0.000            |
|                       | E1    | 0.001                                      | 0.001            | E2    | 0.000                                      | 0.000            |
|                       | E3    | 0.001                                      | 0.001            | E3    | 0.001                                      | 0.001            |
|                       |       |  |                  | E4    | 0.001                                      | 0.001            |
| 100                   | A3    | 201.611                                    | 198.341          | A2    | 200.912                                    | 197.359          |
|                       | G     | 201.602                                    | 198.332          | E1    | 200.903                                    | 197.350          |
|                       | E2    | 201.593                                    | 198.323          | E2    | 200.904                                    | 197.350          |
|                       | E3    | 201.593                                    | 198.323          | E3    | 200.895                                    | 197.341          |
|                       |       |  |                  | E4    | 200.895                                    | 197.341          |
| 010                   | A2    | 241.783                                    | 242.603          | A2    | 241.607                                    | 242.686          |
|                       | G     | 241.774                                    | 242.593          | E1    | 241.598                                    | 242.676          |
|                       | E1    | 241.765                                    | 242.584          | E2    | 241.598                                    | 242.676          |
|                       | E4    | 241.765                                    | 242.584          | E3    | 241.589                                    | 242.667          |
|                       |       |  |                  | E4    | 241.589                                    | 242.667          |
| 200                   | A1    | 391.094                                    | 386.528          | A1    | 389.609                                    | 384.831          |
|                       | G     | 391.225                                    | 386.658          | E1    | 389.732                                    | 384.954          |
|                       | E1    | 391.358                                    | 386.789          | E2    | 389.734                                    | 384.956          |
|                       | E3    | 391.358                                    | 386.789          | E3    | 389.859                                    | 385.081          |
|                       |       |  |                  | E4    | 389.859                                    | 385.081          |
| 001                   | A1    | 412.086                                    | 413.042          | A1    | 409.170                                    | 410.432          |
|                       | G     | 412.086                                    | 413.039          | E1    | 409.173                                    | 410.430          |
|                       | E1    | 412.087                                    | 413.036          | E2    | 409.173                                    | 410.430          |
|                       | E3    | 412.087                                    | 413.036          | E3    | 409.176                                    | 410.428          |
|                       |       |  |                  | E4    | 409.176                                    | 410.428          |
| 110                   | A4    | 422.176                                    | 420.471          | A1    | 421.629                                    | 419.905          |
|                       | G     | 422.393                                    | 420.691          | E1    | 421.846                                    | 420.123          |
|                       | E2    | 422.609                                    | 420.910          | E2    | 421.838                                    | 420.116          |
|                       | E4    | 422.609                                    | 420.910          | E3    | 422.053                                    | 420.333          |
|                       |       |  |                  | E4    | 422.054                                    | 420.333          |
| 020                   | A1    | 480.889                                    | 481.940          | A1    | 479.987                                    | 481.654          |

Table 1—Continued

| $(v_{11} v_{15} v_7)$ | Symm. | $^{12}\text{CH}_3\text{O}^{12}\text{CH}_3$ |                  | Symm. | $^{13}\text{CH}_3\text{O}^{12}\text{CH}_3$ |                  |
|-----------------------|-------|--|------------------|-------|--|------------------|
|                       |       | OLD <sup>a</sup>                           | NEW <sup>b</sup> |       | OLD <sup>c</sup>                           | NEW <sup>b</sup> |
|                       | G     | 480.960                                    | 482.020          | E1    | 480.059                                    | 481.734          |
|                       | E1    | 481.031                                    | 482.099          | E2    | 480.057                                    | 481.731          |
|                       | E3    | 481.031                                    | 482.099          | E3    | 480.129                                    | 481.811          |
|                       |       |  |                  | E4    | 480.129                                    | 481.811          |
| 300                   | A3    | 569.642                                    | 564.130          | A2    | 568.029                                    | 562.043          |
|                       | G     | 567.967                                    | 562.616          | E1    | 566.480                                    | 560.650          |
|                       | E2    | 566.614                                    | 561.352          | E2    | 566.406                                    | 560.592          |
|                       | E3    | 566.615                                    | 561.352          | E3    | 565.143                                    | 559.416          |
|                       |       |  |                  | E4    | 565.143                                    | 559.416          |
| 210                   | A2    | 590.656                                    | 587.974          | A2    | 589.896                                    | 587.047          |
|                       | G     | 588.364                                    | 585.674          | E1    | 587.584                                    | 584.752          |
|                       | E1    | 585.795                                    | 583.182          | E2    | 587.703                                    | 584.850          |
|                       | E4    | 585.797                                    | 583.184          | E3    | 585.152                                    | 582.397          |
|                       |       |  |                  | E4    | 585.153                                    | 582.398          |
| 101                   | A3    | 613.117                                    | 611.569          | A2    | 610.202                                    | 608.235          |
|                       | G     | 613.206                                    | 611.610          | E1    | 610.290                                    | 608.283          |
|                       | E2    | 613.294                                    | 611.643          | E2    | 610.291                                    | 608.286          |
|                       | E3    | 613.294                                    | 611.642          | E3    | 610.379                                    | 608.329          |
|                       |       |  |                  | E4    | 610.378                                    | 608.329          |
| 011                   | A2    | 636.395                                    | 638.255          | A2    | 634.044                                    | 636.816          |
|                       | G     | 636.449                                    | 638.313          | E1    | 634.095                                    | 636.870          |
|                       | E1    | 636.506                                    | 638.371          | E2    | 634.090                                    | 636.867          |
|                       | E4    | 636.507                                    | 638.372          | E3    | 634.144                                    | 636.922          |
|                       |       |  |                  | E4    | 634.144                                    | 636.923          |
| 120                   | A3    | 648.652                                    | 647.438          | A2    | 646.719                                    | 645.721          |
|                       | G     | 647.493                                    | 646.185          | E1    | 645.527                                    | 644.432          |
|                       | E2    | 646.295                                    | 644.894          | E2    | 645.564                                    | 644.471          |
|                       | E3    | 646.286                                    | 644.884          | E3    | 644.328                                    | 643.140          |
|                       |       |  |                  | E4    | 644.319                                    | 643.129          |
| 400                   | A1    | 706.250                                    | 703.223          | A1    | 705.812                                    | 702.388          |
|                       | G     | 708.488                                    | 705.787          | E1    | 707.928                                    | 704.883          |

Table 1—Continued

| $(v_{11} v_{15} v_7)$ | Symm. | $^{12}\text{CH}_3\text{O}^{12}\text{CH}_3$ |                  | Symm. | $^{13}\text{CH}_3\text{O}^{12}\text{CH}_3$ |                  |
|-----------------------|-------|--|------------------|-------|--|------------------|
|                       |       | OLD <sup>a</sup>                           | NEW <sup>b</sup> |       | OLD <sup>c</sup>                           | NEW <sup>b</sup> |
|                       | E1    | 727.268                                    | 723.674          | E2    | 708.391                                    | 705.332          |
|                       | E3    | 726.577                                    | 722.224          | E3    | 726.116                                    | 722.212          |
|                       |       |  |                  | E4    | 725.509                                    | 720.574          |
| 030                   | A2    | 717.917                                    | 718.784          | A2    | 716.038                                    | 718.141          |
|                       | G     | 717.442                                    | 718.122          | E1    | 715.594                                    | 717.483          |
|                       | E1    | 716.716                                    | 716.717          | E2    | 715.601                                    | 717.481          |
|                       | E4    | 717.059                                    | 717.671          | E3    | 714.923                                    | 715.883          |
|                       |       |  |                  | E4    | 715.225                                    | 717.040          |
| 310                   | A4    | 711.733                                    | 709.884          | A1    | 711.676                                    | 709.692          |
|                       | G     | 731.779                                    | 728.819          | E1    | 731.382                                    | 728.093          |
|                       | E2    | 735.657                                    | 733.397          | E2    | 730.719                                    | 727.475          |
|                       | E4    | 736.031                                    | 733.928          | E3    | 735.199                                    | 732.699          |
|                       |       |  |                  | E4    | 735.531                                    | 733.219          |
| 220                   | A1    | 785.149                                    | 779.346          | A1    | 783.614                                    | 777.555          |
|                       | G     | 784.508                                    | 779.640          | E1    | 783.133                                    | 778.089          |
|                       | E1    | 783.988                                    | 779.822          | E2    | 783.084                                    | 778.032          |
|                       | E3    | 783.912                                    | 779.724          | E3    | 782.666                                    | 778.371          |
|                       |       |  |                  | E4    | 782.595                                    | 778.274          |
| 002                   | A1    | 805.550                                    | 806.600          | A1    | 800.434                                    | 802.112          |
|                       | G     | 805.861                                    | 806.826          | E1    | 800.978                                    | 802.594          |
|                       | E1    | 806.194                                    | 807.097          | E2    | 800.964                                    | 802.564          |
|                       | E3    | 806.105                                    | 806.966          | E3    | 801.516                                    | 803.083          |
|                       |       |  |                  | E4    | 801.443                                    | 802.962          |
| 130                   | A4    | 810.976                                    | 810.464          | A1    | 809.108                                    | 808.658          |
|                       | G     | 809.429                                    | 808.742          | E1    | 807.652                                    | 807.050          |
|                       | E2    | 807.515                                    | 806.719          | E2    | 807.701                                    | 807.095          |
|                       | E4    | 807.579                                    | 806.834          | E3    | 805.916                                    | 805.227          |
|                       |       |  |                  | E4    | 805.970                                    | 805.333          |
| 201                   | A1    | 823.691                                    | 824.164          | A1    | 819.009                                    | 819.193          |
|                       | G     | 822.370                                    | 822.840          | E1    | 818.451                                    | 818.710          |
|                       | E1    | 821.995                                    | 822.630          | E2    | 818.364                                    | 818.633          |

Table 1—Continued

| $(v_{11} v_{15} v_7)$    | Symm. | $^{12}\text{CH}_3\text{O}^{12}\text{CH}_3$ |                  | Symm. | $^{13}\text{CH}_3\text{O}^{12}\text{CH}_3$ |                  |
|--------------------------|-------|--|------------------|-------|--|------------------|
|                          |       | OLD <sup>a</sup>                           | NEW <sup>b</sup> |       | OLD <sup>c</sup>                           | NEW <sup>b</sup> |
|                          | E3    | 821.689                                    | 822.259          | E3    | 818.138                                    | 818.488          |
|                          |       |  |                  | E4    | 817.920                                    | 818.254          |
| Unlabelled energy levels |       | ⋮  | ⋮                |       | ⋮  | ⋮                |
| 0 2 1 <sup>d</sup>       | A1    | 858.148                                    | 860.357          | A1    | 855.085                                    | 858.393          |
|                          | G     | 857.950                                    | 860.106          | E1    | 854.896                                    | 858.156          |
|                          | E1    | 857.832                                    | 859.899          | E2    | 854.913                                    | 858.173          |
|                          | E3    | 857.778                                    | 859.845          | E3    | 854.795                                    | 857.961          |
|                          |       |  |                  | E4    | 854.746                                    | 857.914          |

<sup>a</sup>Calculated with the adjusted Hamiltonian of Villa et al. (2011).

<sup>b</sup>Calculated with the refined Hamiltonian of this work.

<sup>c</sup>Calculated with the adjusted Hamiltonian of Carvajal et al. (2012).

<sup>d</sup>Tentative label.

Table 2. APPENDIX: Experimental and calculated wavenumbers ( $\text{cm}^{-1}$ ) of the Raman transitions of DME and  $^{13}\text{C}$ -DME.

| Band # | $(v_{11} v_{15} v_7)_i \rightarrow (v_{11} v_{15} v_7)_f$ | Symm. | $^{12}\text{CH}_3\text{O}^{12}\text{CH}_3$ |                   | Symm. | $^{13}\text{CH}_3\text{O}^{12}\text{CH}_3$ |                   |
|--------|---|-------|--|-------------------|-------|--|-------------------|
|        |   |       | Calc. <sup>a</sup>                         | Exp. <sup>b</sup> |       | Calc. <sup>a</sup>                         | Exp. <sup>b</sup> |
| 1      | 000 $\rightarrow$ 100                                     | A3    | 198.34                                     | $197.8 \pm 0.2$   | A2    | 197.36                                     | -                 |
|        |   | G     | 198.33                                     |                   | E1    | 197.35                                     |                   |
|        |   | E2    | 198.32                                     |                   | E2    | 197.35                                     |                   |
|        |   | E3    | 198.32                                     |                   | E3    | 197.34                                     |                   |
|        |   |       |  |                   | E4    | 197.34                                     |                   |
| 2      | 000 $\rightarrow$ 010                                     | A2    | 242.60                                     | $241.4 \pm 0.4$   | A2    | 242.69                                     | $241.4 \pm 0.5$   |
|        |   | G     | 242.59                                     |                   | E1    | 242.68                                     |                   |
|        |   | E1    | 242.58                                     |                   | E2    | 242.68                                     |                   |
|        |   | E4    | 242.58                                     |                   | E3    | 242.67                                     |                   |
|        |   |       |  |                   | E4    | 242.67                                     |                   |
| 3      | 000 $\rightarrow$ 200                                     | A1    | 386.53                                     | $385.2 \pm 0.2$   | A1    | 384.83                                     | $385.0 \pm 0.2$   |
|        |   | G     | 386.66                                     |                   | E1    | 384.95                                     |                   |
|        |   | E1    | 386.79                                     |                   | E2    | 384.96                                     |                   |
|        |   | E3    | 386.79                                     |                   | E3    | 385.08                                     |                   |
|        |   |       |  |                   | E4    | 385.08                                     |                   |
| 4      | 100 $\rightarrow$ 300                                     | A3    | 365.79                                     | $362.6 \pm 0.2$   | A2    | 364.68                                     | $362.3 \pm 0.2$   |
|        |   | G     | 364.28                                     |                   | E1    | 363.30                                     |                   |
|        |   | E2    | 363.03                                     |                   | E2    | 363.24                                     |                   |
|        |   | E3    | 363.03                                     |                   | E3    | 362.08                                     |                   |
|        |   |       |  |                   | E4    | 362.08                                     |                   |
| 5      | 001 $\rightarrow$ 201                                     | A1    | 411.12                                     | $411.1 \pm 0.2$   | A1    | 408.76                                     | $409.3 \pm 0.2$   |
|        |   | G     | 409.80                                     |                   | E1    | 408.28                                     |                   |
|        |   | E1    | 409.59                                     |                   | E2    | 408.20                                     |                   |
|        |   | E3    | 409.22                                     |                   | E3    | 408.06                                     |                   |
|        |   |       |  |                   | E4    | 407.83                                     |                   |
| 6      | 000 $\rightarrow$ 020                                     | A1    | 481.94                                     | $482.0 \pm 0.2$   | A1    | 481.65                                     | $481.1 \pm 0.2$   |
|        |   | G     | 482.02                                     |                   | E1    | 481.73                                     |                   |
|        |   | E1    | 482.10                                     |                   | E2    | 481.73                                     |                   |
|        |   | E3    | 482.10                                     |                   | E3    | 481.81                                     |                   |
|        |   |       |  |                   | E4    | 481.81                                     |                   |
| 7      | 100 $\rightarrow$ 120                                     | A3    | 449.10                                     | $450.2 \pm 0.4$   | A2    | 448.36                                     | $449.2 \pm 0.5$   |

Table 2—Continued

| Band # | $(v_{11} v_{15} v_7)_i \rightarrow (v_{11} v_{15} v_7)_f$ | Symm. | $^{12}\text{CH}_3\text{O}^{12}\text{CH}_3$ |                   | Symm. | $^{13}\text{CH}_3\text{O}^{12}\text{CH}_3$ |                   |
|--------|---|-------|--|-------------------|-------|--|-------------------|
|        |   |       | Calc. <sup>a</sup>                         | Exp. <sup>b</sup> |       | Calc. <sup>a</sup>                         | Exp. <sup>b</sup> |
|        |   | G     | 447.85                                     |                   | E1    | 447.08                                     |                   |
|        |   | E2    | 446.57                                     |                   | E2    | 447.12                                     |                   |
|        |   | E3    | 446.56                                     |                   | E3    | 445.80                                     |                   |
|        |   |       |  |                   | E4    | 445.79                                     |                   |
| 8      | 010 → 030   | A2    | 476.18                                     | 480.7 ± 0.2       | A2    | 475.46                                     | 479.0 ± 0.3       |
|        |   | G     | 475.53                                     |                   | E1    | 474.81                                     |                   |
|        |   | E1    | 474.13                                     |                   | E2    | 474.81                                     |                   |
|        |   | E4    | 475.09                                     |                   | E3    | 473.22                                     |                   |
|        |   |       |  |                   | E4    | 474.37                                     |                   |
| 9      | 000 → 001   | A1    | 413.04                                     | 412.5 ± 0.2       | A1    | 410.43                                     | 410.0 ± 0.2       |
|        |   | G     | 413.04                                     |                   | E1    | 410.43                                     |                   |
|        |   | E1    | 413.04                                     |                   | E2    | 410.43                                     |                   |
|        |   | E3    | 413.04                                     |                   | E3    | 410.43                                     |                   |
|        |   |       |  |                   | E4    | 410.43                                     |                   |
| 10     | 100 → 101   | A3    | 413.23                                     | 413.2 ± 0.2       | A2    | 410.88                                     | 410.8 ± 0.2       |
|        |   | G     | 413.28                                     |                   | E1    | 410.93                                     |                   |
|        |   | E2    | 413.32                                     |                   | E2    | 410.94                                     |                   |
|        |   | E3    | 413.32                                     |                   | E3    | 410.99                                     |                   |
|        |   |       |  |                   | E4    | 410.99                                     |                   |
| 11     | 010 → 011   | A2    | 395.65                                     | 395.5 ± 0.2       | A2    | 394.13                                     | 393.9 ± 0.2       |
|        |   | G     | 395.72                                     |                   | E1    | 394.19                                     |                   |
|        |   | E1    | 395.79                                     |                   | E2    | 394.19                                     |                   |
|        |   | E4    | 395.79                                     |                   | E3    | 394.26                                     |                   |
|        |   |       |  |                   | E4    | 394.26                                     |                   |
| 12     | 200 → 002   | A1    | 420.07                                     | 424.2 ± 0.2       | A1    | 417.28                                     | 422.0 ± 0.3       |
|        |   | G     | 420.17                                     |                   | E1    | 417.64                                     |                   |
|        |   | E1    | 420.31                                     |                   | E2    | 417.61                                     |                   |
|        |   | E3    | 420.18                                     |                   | E3    | 418.00                                     |                   |
|        |   |       |  |                   | E4    | 417.88                                     |                   |
| 13     | 200 → 201   | A1    | 437.64                                     | 437.5 ± 0.5       | A1    | 434.36                                     | 434.0 ± 0.2       |
|        |   | G     | 436.18                                     |                   | E1    | 433.76                                     |                   |

Table 2—Continued

| Band # | $(v_{11} v_{15} v_7)_i \rightarrow (v_{11} v_{15} v_7)_f$ | Symm. | $^{12}\text{CH}_3\text{O}^{12}\text{CH}_3$ |                   | Symm. | $^{13}\text{CH}_3\text{O}^{12}\text{CH}_3$ |                   |
|--------|---|-------|--|-------------------|-------|--|-------------------|
|        |   |       | Calc. <sup>a</sup>                         | Exp. <sup>b</sup> |       | Calc. <sup>a</sup>                         | Exp. <sup>b</sup> |
|        |   | E1    | 435.84                                     |                   | E2    | 433.68                                     |                   |
|        |   | E3    | 435.47                                     |                   | E3    | 433.41                                     |                   |
|        |   |       |  |                   | E4    | 433.17                                     |                   |
| 14     | 001 → 002   | A1    | 393.56                                     | 396.3 ± 0.3       | A1    | 391.68                                     | 394.7 ± 0.2       |
|        |   | G     | 393.79                                     |                   | E1    | 392.16                                     |                   |
|        |   | E1    | 394.06                                     |                   | E2    | 392.13                                     |                   |
|        |   | E3    | 393.93                                     |                   | E3    | 392.66                                     |                   |
|        |   |       |  |                   | E4    | 392.53                                     |                   |
| 15     | 020 → 021 <sup>c</sup>                                    | A1    | 378.42                                     | 381.0 ± 0.2       | A1    | 376.74                                     | 379.2 ± 0.2       |
|        |   | G     | 378.09                                     |                   | E1    | 376.42                                     |                   |
|        |   | E1    | 377.80                                     |                   | E2    | 376.44                                     |                   |
|        |   | E3    | 377.75                                     |                   | E3    | 376.15                                     |                   |
|        |   |       |  |                   | E4    | 376.10                                     |                   |

<sup>a</sup>Calculated with the refined Hamiltonian of this work.

<sup>b</sup>Experimental.

<sup>c</sup>Tentative assignment.

Table 3. APPENDIX: Expansion Coefficients for the refined CCSD(T)/aug-cc-pVTZ effective Potential Energy Surface of  $^{12}\text{CH}_3\text{O}^{12}\text{CH}_3$  and  $^{13}\text{CH}_3\text{O}^{12}\text{CH}_3$ .

| Coeff. <sup>a</sup> | $^{12}\text{CH}_3\text{O}^{12}\text{CH}_3$ | $^{13}\text{CH}_3\text{O}^{12}\text{CH}_3$ |
|---------------------|--|--|
|                     | $V^{\text{eff}}$ <sup>b</sup>              | $V^{\text{eff}}$ <sup>b</sup>              |
| $A_{000}$           | 970.1546                                   | 970.1576                                   |
| $A_{100}$           | -54.6202                                   | -54.7897                                   |
| $A_{200}$           | 10.2064 <sup>fitted</sup>                  | 10.2329 <sup>fitted</sup>                  |
| $A_{300}$           | -0.1424                                    | -0.1402                                    |
| $A_{010}$           | -495.2177                                  | -497.1729                                  |
| $A_{110}$           | 31.7310                                    | 31.7310                                    |
| $A_{210}$           | -1.0805                                    | -1.0805                                    |
| $A_{310}$           | 0.0134                                     | 0.0134                                     |
| $A_{011}$           | 25.4803                                    | 26.7661                                    |
| $A_{111}$           | -12.7102                                   | -12.7102                                   |
| $A_{211}$           | 0.5208                                     | 0.5208                                     |
| $A_{311}$           | -0.0056                                    | -0.0056                                    |
| $A_{020}$           | -1.8845 <sup>fitted</sup>                  | -0.9984 <sup>fitted</sup>                  |
| $A_{120}$           | 1.1183                                     | 1.1183                                     |
| $A_{220}$           | -0.1071                                    | -0.1071                                    |
| $A_{320}$           | 0.0038                                     | 0.0038                                     |
| $A_{021}$           | 0.7500                                     | 0.8149                                     |
| $A_{121}$           | -0.3289                                    | -0.3289                                    |
| $A_{221}$           | 0.0481                                     | 0.0481                                     |
| $A_{321}$           | -0.0026                                    | -0.0026                                    |
| $A_{022}$           | 1.7800                                     | 1.3639                                     |
| $A_{122}$           | -0.0958                                    | -0.0958                                    |
| $A_{222}$           | -0.0293                                    | -0.0293                                    |
| $A_{322}$           | 0.0026                                     | 0.0026                                     |
| $B_{011}$           | -13.9554                                   | -15.8995                                   |
| $B_{111}$           | 14.3670                                    | 14.3670                                    |
| $B_{211}$           | -0.7375                                    | -0.7375                                    |
| $B_{311}$           | 0.0117                                     | 0.0117                                     |

<sup>a</sup>Expansion coefficients  $A_{lmn}$  and  $B_{lmn}$  (in units of  $\text{cm}^{-1}/\text{degrees}^l$ ) of Eq. (3).

<sup>b</sup>Refined effective potential parameters. Fitted parameters are indicated.